39th IAHR WORLD CONGRESS GRANADA, SPAIN 2022 From Snow to Sea 19-24 June 2022

Proceedings of the 39th IAHR World Congress
19–24 June 2022, Granada, Spain
doi://10.3850/IAHR-39WC2521716X2022573

Laser Triangulation-Based Ranging of Turbulent Water Surface with Epipolar Lines

Urban Pavlovčič [(1)], Gašper Rak [(2)], Marko Hočevar [(3)] and Matija Jezeršek [(1)]

[(1)] University of Ljubljana, Faculty of Mechanical Engineering, Laboratory of Laser Techniques, Ljubljana, Slovenia
[(2)] University of Ljubljana, Faculty for Civil and Geodetic Engineering, Chair of Fluid Mechanics, Ljubljana, Slovenia
[(3)] University of Ljubljana, Faculty of Mechanical Engineering, Laboratory for Hydraulic Machines, Ljubljana, Slovenia
e-mail: gasper.rak@fgg.uni-lj.si

Abstract

Complex hydraulic phenomena in terms of high-speed flow and particularly air flow features are expected as future challenges in hydraulic structure design and the main research topics. Accurate and reliable measurements that provide new information and knowledge about phenomena and processes as well as quality data for calibration and verification of numerical models are crucial. This paper presents the applicability of laser triangulation-based ranging of turbulent water surface with epipolar lines for enhanced spatial resolution. The experiment was conducted on the measuring station of supercritical junction flow, where distinctively 3D, turbulent, two-phase flow occurs. The system for acquisition of transversal profile of the water surface and the range of water surface fluctuation was composed of a LIDAR device as light source only, and a high-speed camera with frame rate of 100 kfps. Since the light reflection from the water surface is far more complex compared to the one from a diffuse surface, single point illumination was used. The approach enables application of the epipolar lines in the image post-processing and more efficient distinction between primary reflection, used for water surface ranging, and secondary reflections, which introduce noise in the measurements and consequently increase measuring uncertainty.

Keywords: Turbulent water flow; Water surface ranging; Laser triangulation; LIDAR

1. INTRODUCTION

Measurements of free surface flows are important in a wide range of water engineering application in order to understand these flows and validate predictive tools we need to measure the free surface elevation accurately. It is also important for mechanical engineering, since water surface fluctuations affect the boundary conditions of mechanical equipment.

The water/air interface has been studied experimentally, numerically and theoretically over the last few decades, and a good overview is given by H. Chanson (2013). One of methods used for measuring water surface shape is Light Detection And Ranging (LIDAR), which is based on point-wise laser light illumination of the water surface and detection of reflected light, where the temporal intensity profile is analyzed. Since the measuring frequency and laser beam scanning speed can be in order of 100 kHz and more than 500 profiles/second, the water surface dynamics can be measured with a reasonably high resolution. Rak et al. (2018) took measurements of aerated confluence flow using LIDAR and showed that laser scanning can provide accurate measurements of free-water surface topography in cases where highly aerated flow is present. Kramer et al. (2020) studied the suitability of LIDAR in high-velocity air–water flows on stepped spillways, while others have used LIDAR to characterize water surfaces using LIDAR based bathymetry (Westfeld et al. 2017). Montano et al. (2018) analyzed free-surface profiles in aerated hydraulic jumps for high Fr numbers. They used raw LIDAR data to calculate time averaged free-surface profiles and standard deviation and estimate frequency spectra of free-surface fluctuations.

Laser triangulation measurements of surfaces are common, but work relating to making triangulation surface water measurements of highly turbulent and aerated flows is at best limited (Amann et al., 2001). Mulsow et al. (2006, 2008) used a modified triangulation method capable of measuring a reflected laser line. Other optical methods, such as particle image velocimetry and stereo vision photogrammetry or acoustic methods like Doppler velocimetry are more common but fail to provide measurements for highly aerated turbulent flows (Brazhnikov et al., 2002).

The main problem using any of the before mentioned optical methods for measuring aerated water surface lies in complex light reflection from the surface. Since the light is reflected and also transmitted on any interface between optical media with different refractive indices, the image of surface illuminated by the spot laser light is normally much wider and irregular than in case of illuminated diffuse nontransparent surface and the light path distance can be also significantly longer in case of multiple reflections. Consequently, the

measured distance includes also a part which approximately corresponds to the light mean penetration depth, which depends mostly on water aeration level.

In this study, a laser profilometer using a high-speed camera and based on the triangulation principle was used to measure the height of turbulent water surfaces with highly-aerated, supercritical flows. The novel approach of the epipolar line was applied to surpass weaknesses of the optical methods and enhancing the spatial resolution of triangulation measurement (Zhang, 2013). The results show that parameters of the algorithm, developed for analysis of free-water-surfaces based on the laser triangulation, have almost an order of magnitude smaller influence than the measuring uncertainty of the applied measuring system.

2. EXPERIMENT SET-UP AND MEASUREMENTS

2.1 Measuring System

The T-shaped junction, with a 90° angle between the axis of the main channel and its side inflow, has a 6-m long main channel and a 1-m long side channel. The experimental apparatus was entirely made of glass, which reduced the effect of walls on flow conditions as well allowed for a side view of the flow conditions. A horizontal bottom of all sections was provided to optimize the measurements and particularly to allow for appropriate inflows to the model, to minimize the number of joints at the confluence that might bring additional disturbances, and to reach the desired water flow velocities at the channels. No additives were put into water to increase diffuse reflectance of the water.

Main flow rate was 35.5 l/s at height 20 mm with Reynolds number $7.1 \cdot 10^4$ and Froude number 8, while tributary flow rate was 26.6 l/s at height of 20 mm, with Reynolds number $5.3 \cdot 10^4$ and Froude number 6.

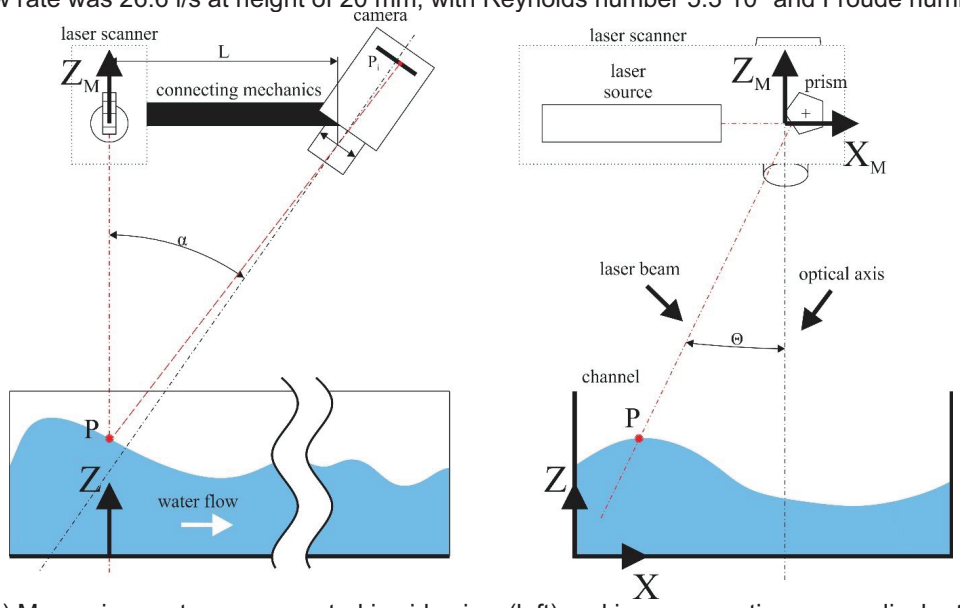

Figure 1. a) Measuring system represented in side view (left) and in cross-section perpendicular to the water flow direction (right)

The measuring devices were mounted on the frame construction 100 cm above the bottom of the channel and 100 cm downstream from the junction. Setup was composed of three main components: laser scanner, high-speed camera and connecting mechanics, to which the scanner and the camera were firmly attached. A LIDAR instrument LMS400 manufactured by SICK AG was used as the light source only. The laser scanner operates in the visible red-light wavelength λ = 650 nm. It is used for both indoor and industrial use with distances not exceeding 7 m. The instrument allows for a selection of the combination of scanning frequency 270–500 Hz and an angular resolution from 0.1° to 1.0°. For an optimum number of the measured reflections in the individual recordings of cross-sections we used a frequency of 269.8 Hz and an angular resolution of 0.2. Single laser point illumination was chosen over laser line illumination since it is possible to determine the course of the epipolar line and in that manner eliminate side reflections.

As high-speed camera was used, the Photron FASTCAM SA-Z, type 2100K-M-64GB. It was mounted at α = 55° relative to the scanning sheet of the laser scanner to capture images. A resolution of the captured images was set to 640x280 pixels and frame rate to 100 kfps. Shutter time was set to 8 μs. Measurement process lasted about 2.1 s, so that 255 627 images were captured, so that 543 profiles were captured.

The system was calibrated using solid, diffuse surfaces.

2.2 Image Processing

Procedure of image post-processing consists of 6 steps. A detailed description is given in a scientific paper (Pavločič at el., 2020) and could be summarized as follows:

1) Individual image of sequence was identified as relevant and irrelevant image, considering where the laser beam illuminates the water surface. Only images with the number of pixels above the threshold were considered as relevant. Typically, there were 112 images for each scan line. On the first image of the transition, the laser beam was located on the left edge of the water channel, and on the last image of the transition the laser dot was located on the right edge. Due to the filtering and area surrounding the epipolar line some defects may occur when the distance between the laser dot and glass side of the channel is smaller than the width of the area or filter width. Positioning accuracy could be affected by consecutive reflections of laser beam that may occur on the turbulent and complex aerated water surface. That is why we took advantage of the principle of the epipolar line, which represents the line along which the intersection between the laser beam and water may occur at any given time (Zhang, 2013).
2) Detected laser spots were grouped by each angle of illumination and an epipolar line was fitted to each group. The optimal intersection of all these lines was determined as a rotational axis of the epipolar line. The values of the angle were filtered using the moving average filter.
3) The image was filtered using a Gaussian filter and the location of the reflected laser dot was found as the pixel of the maximal intensity inside the defined distance around the epipolar line.
4) Detection of actual location of the laser dot and calculation of the ideal location as a perpendicular projection of laser dot onto the epipolar line.
5) Calculation of laser spot location in 3D space using triangulation method.
6) Reconstruction of 3D profiles and their translation from camera coordinate system to global one.

Figure 2 presents a small part of the image and specular reflections of laser beam on water surface of the aerated flow. Although six dots might be seen, only three of them were considered valid, namely ones located inside the epipolar line region (marked with red dotted lines). Dots outside of the region are marked with red arrows, while dots inside are marked yellow arrows. The brightest one (green arrow) is considered the primary reflection and used in further calculations.

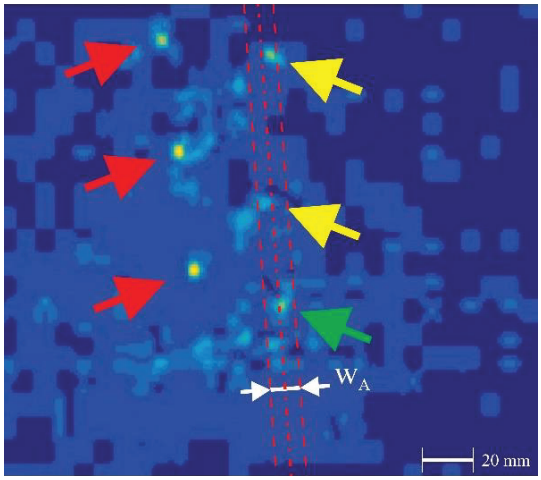

Figure 2. Example of complex laser beam reflection from aerated water surface. Detected point is shown with a green arrow. Two other laser dots lie within the epipolar line region, while three of them (red arrows) lie outside and are excluded from searching for maximal intensity.

2.3 Experimental Methods

Despite highly turbulent aerated flow its dynamics across the measured cross-section varied. From figure 3 we could distinguish much rougher water surface on the left side of the flume and smoother on the right one. For further analysis a representative section of rougher water surface was determined X_1 = 100 mm and X_2 = 150 mm, and area between X_3 = 400 mm and X_4 = 450 mm as a representative of smoother water surface.

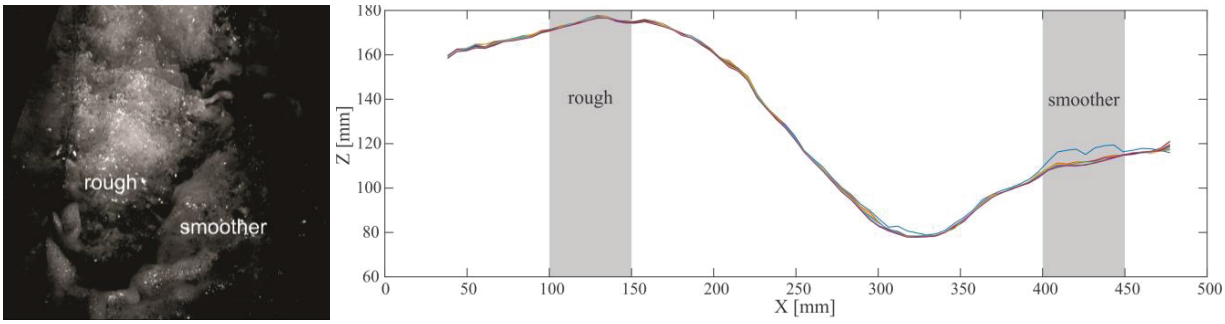

Figure 3. Sample image of water surface (left), and rough and smoother regions (right).

An analysis of the parameters´ influence on results of the proposed algorithm was separately conducted for sections of *rough* and *smoother* water surface. Each parameter was varied inside a certain interval and resulting average profiles were calculated. Scatter among these profiles served as an estimator of parameter's influence. Analyzed parameters were:

- width of filtering kernel (w_K), when *actual* location of laser dot is searched,
- height of filtering kernel (h_K), when *actual* location of laser dot is searched,
- width of the area surrounding the epipolar line (w_A), where maximal intensity is searched.

3. RESULTS AND DISCUSSION

The magnification of the camera was not constant across the entire measuring range, and therefore dimensions in pixels don't correspond directly to distances in the experiment. Therefore, all the parameters are referred to in pixel units, while distances in the experiment are referred to in millimeters (i.e. one pixel roughly corresponds to between 1.0 mm and 1.4 mm).

3.1 Width of Filtering Kernel

The influence of the width of filtering kernel on the results was evaluated with varying it from 1 to 21 pix, with step of 2 pix, while procedure was conducted as described before. Filter height and w_A were constant and set at 5 pix. In figure 4 the results are separately shown for rough and smooth water surfaces.

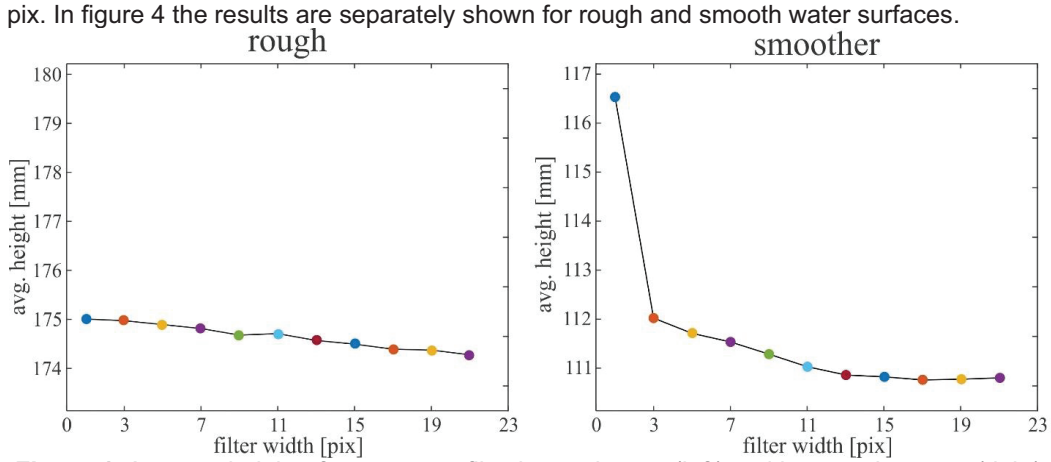

Figure 4. Average height of average profiles in rough area (left) and in smoother area (right).

Comparison of water surface profiles for different values of width of filtering kernel showed no significant deviations. Average scatter is 0.76 mm. The greatest difference was observed for a filter width of 1 pix, so the outlier corresponds to the profile, reconstructed with filter width of 1 pix. If the outlier is removed the average scatter drops to 0.52 mm. Increasing the filter width results in decreasing profile height, though drop is small, namely 0.73 mm and 1.20 mm in rough water flow and smoother flow, respectively. Since more scattering is included in case of larger kernel, peak location is detected a bit lower.

3.2 Height of Filtering Kernel

Similar analysis was performed for the height of the kernel (h_H). The height was increasing in the same range with the same step, while the widths (w_H and w_A) were constant and set at 5 pix. In this case the

average scatter was 0.91 mm. For the rough water surface (Figure 5, left) no trend can be observed. Differences between lowest and highest point, and difference between smallest and biggest filter height were 0.16 mm and 0.09 mm, respectively. For the smoother water surface, a lowering trend could be observed for larger filter heights. It is also more distinguished than it was for varying filter width.

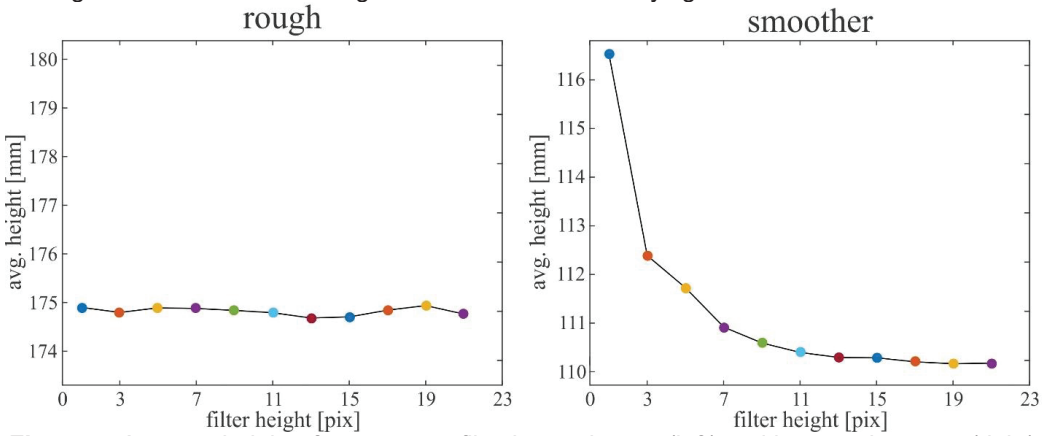

Figure 5. Average height of average profiles in rough area (left) and in smoother area (right).

A similar decreasing trend could be seen for water height, since it is more evident for smoother water surface. In the section of the rough water surface the difference between the smallest and biggest filter height was 0.09 mm, while in case of smoother water the difference between the biggest and smallest filter height is more significant, 2.19 mm.

3.3 Width of the Area Surrounding the Epipolar Line

Values of the width of the area surrounding the epipolar line were varying between 1 pix and 11 pix, with increment of 1 pix, while kernel dimensions were set to 5 pix. Opposite to previous analysis no outliers were observed as well as height of the surface is increasing (Figure 6). Average deviation between profiles is 0.67 mm. Considering the rougher water surface the difference between lowest and highest point is 0.94 mm, while the increase of 0.66 mm occurs between using the smallest and biggest area width. For the section of the smoother surface the increasing trend is more evident, 1.41 mm from the smallest to biggest area width.

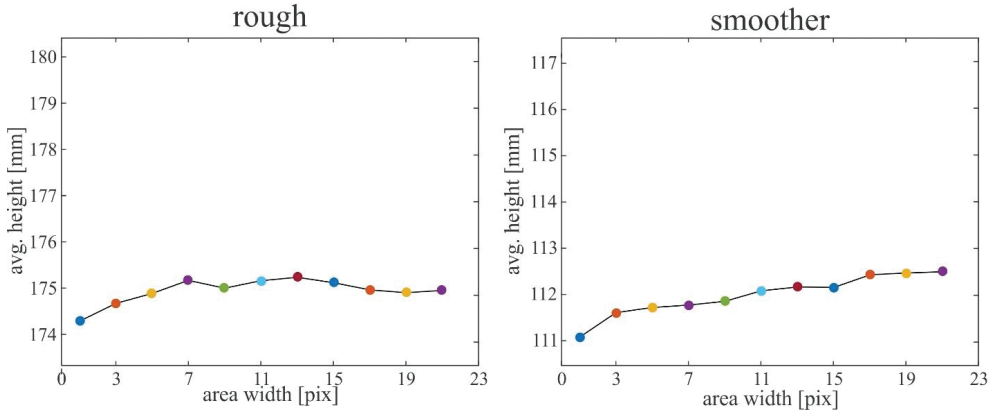

Figure 6. Average height of average profiles in rough area (left) and in smoother area (right).

Figure 7 shows the influence of the analyzed parameters on the number of detected points along the entire cross-section. The influence is given as the ratio of the valid point to all points. With the increase of the filter kernel dimensions, the number of valid points decreases by 3 % and 2 % for increasing height and width, respectively. The reason lies in the decrease of the peak intensity as a consequence of the increase in kernel dimension. Since the threshold value was set as constant, the peak intensity could fall below it. Extending the search area surrounding the epipolar line up to 5 pix results in the increase of the valid points number, but for the dimensions greater than 5 pix, the number of valid points stays more or less the same.

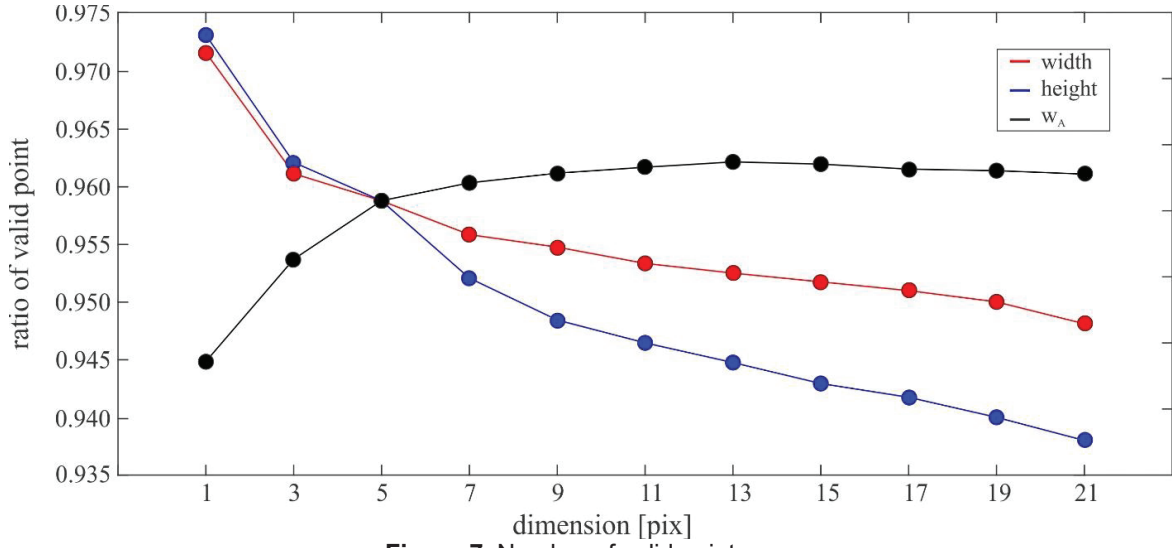

Figure 7. Number of valid points.

4. CONCLUSIONS

The paper presents a non-intrusive measuring method for analysis of the turbulent, aerated water surface. The measuring system and post-processing algorithm is based on the laser triangulation and can measure up to 100 000 points per second. The results of the analysis show the influence of the algorithm's parameters on an average water surface profile. It is almost an order of magnitude smaller than the measuring uncertainty of the applied measuring system. Due to the lack of methods capable of performing measurements of the turbulent, aerated water flow, with comparable spatial and temporal resolution, no reference value for comparison was available. We successfully distinguished between primary and secondary reflections, and eliminated a portion of the latter by the introduction of the epipolar line in the image-processing. Anyway, secondary reflections that lie on the epipolar line cannot be distinguished.

Compared to LIDAR, which has proved in recent years as an efficient measuring method for acquisition of turbulent, two-phase flow profile, our approach rejects reflections outside the epipolar line. While LIDAR uses a frequency modulation approach to improve measuring precision and a measured value is determined as the average of all reflections inside its field of view, the proposed method considers the brightest reflection.

5. ACKNOWLEDGEMENTS

The authors acknowledge the financial support from the Slovenian Research Agency (research core funding No. P2-0167, P2-0180, and P2-0270).

6. REFERENCES

Amann, M.C., Bosch, T., Lescure, M. and Myllylä, R., Rioux. M. (2001). Laser raging: a critical review of usual techniques for distance measurement, *Optical Engineering*, 40 (1): 10-19.

Brazhnikov, M.Y. Kolmakov, G.V. Levchenko, A.A. and Mezhov-Deglin L.P. (2002). Observation of capillary turbulence on the water surface in a wide range of frequencies, *EPL (Europysics Letters)*, 5 (4): 510-516.

Chanson. H. (2013). Hydraulics of Aerated Flows: Qui Pro Quo? *J. Hydraul. Res.*, 51 (3), 223-243.

Kramer, M., H. Chanson, and S. Felder. 2020. Can we improve the nonintrusive characterization of high-velocity air–water flows? Application of LIDAR technology to stepped spillways. *J. Hydraul. Res.,* 58 (2): 1–13.

Mignot, E., Riviere, N. Perkins, R. and Paquier. A. (2008). Flow patterns in a four-batch junction with supercritical flow. *Journal of Hydraulics Engineering*, 134 (6): 701-713.

Montano, L., L. Rui, and S. Felder. (2018). Continuous measurements of time-varying free-surface profiles in aerated hydraulic jumps with a LIDAR. Exp. *Therm Fluid Sci.* 93: 379–397. https://doi.org/10.1016/j.expthermflusci.2018.01.016.

Mulsow, C. Schulze, M. and Westfeld. P. (2006). An optical triangulation method for height measurements on non-stationary water surfaces, International Archives of the Photogrammetry, *Remote Sensing and Spatial Information Sciences*: 2013-2017.

Mulsow, C., Mass, H.G. Westfeld, P. and Schulze M. (2008). Triangulation methods for height profile measurements on instationary water surfaces, *Journal of Applied Geodesy*, 2 (1): 21-29.

Pavlovčič, U., Rak, G., Hočevar, M., Jezeršek, M. (2020). Ranging of Turbulent Water Surfaces Using a Laser Triangulation Principle in a Laboratory Environment. *J. Hydraul. Eng.,* 146 (8): 04020052. https://doi.org/10.1061/(ASCE)HY.1943-7900.0001777

Rak, G., Hočevar, M. and F. Steinman. (2018). Construction of Water Surface Topography using LIDAR Data, *J. Eng. Mech.*, 64 (9): 555-565. 10.5545/sv-jme.2017.4619

Rak, G., Hočevar, M. and F. Steinman, Dular, M., Jezeršek, M. and Pavlovčič, U. (2020). Laser ranging measurements of turbulent water surfaces. *Eur. J. Mech. B Fluids* 81, 165 - 172. 10.1016/j.euromechflu.2020.02.001

Westfeld, P., Maasa, H.G., Richter, K. and Weiss R. (2017). Analysis and correction of ocean wave pattern induced systematic coordinate errors in airborne LiDAR bathymetry, ISPRS *J. Photogramm. Remote Sens.*, 128: 314-325.

Zhang, S. (2013). Handbook of 3D Machine Vision: Optical Metrology and Imaging, 1st ed.: 414 pp.

